Supplement of

Quantitative Precipitation Estimation from Fengyun-4 Geostationary Satellite Multispectral Information, Physical Variables and High-density Meteorological Observations: A Random Forest Model Framework

Xinyan Li, Yuanjian Yang, Jiaqin Mi, Xueyan Bi, You Zhao, Zehao Huang, Chao Liu, Lian Zong, and Wanju Li

Correspondence to: Yuanjian Yang (yyj1985@nuist.edu.cn)

Figures and Tables

Table S1:Wavelengths of the 14 channels of the Fengyun-4 satellite and their application

Channel	NO.	Band(μm)	Application
Visible&Near-Infrared	1	0.47	Cloud,Aerosol
	2	0.65	Cloud,Snow
	3	0.825	Cloud,Aerosol,Vegetation
	4	1.375	Cirrus
	5	1.61	Cloud,Snow
	6	2.25	Cirrus,Aerosol
Shortwave Infrared	7	3.75H	Fire
	8	3.75L	Clouds,Fog
Water Vapor	9	6.25	WV
	10	7.1	WV
Longwave Infrared	11	8.5	Sand dust
	12	10.7	Cloud
	13	12.0	Cloud
	14	13.5	Cloud

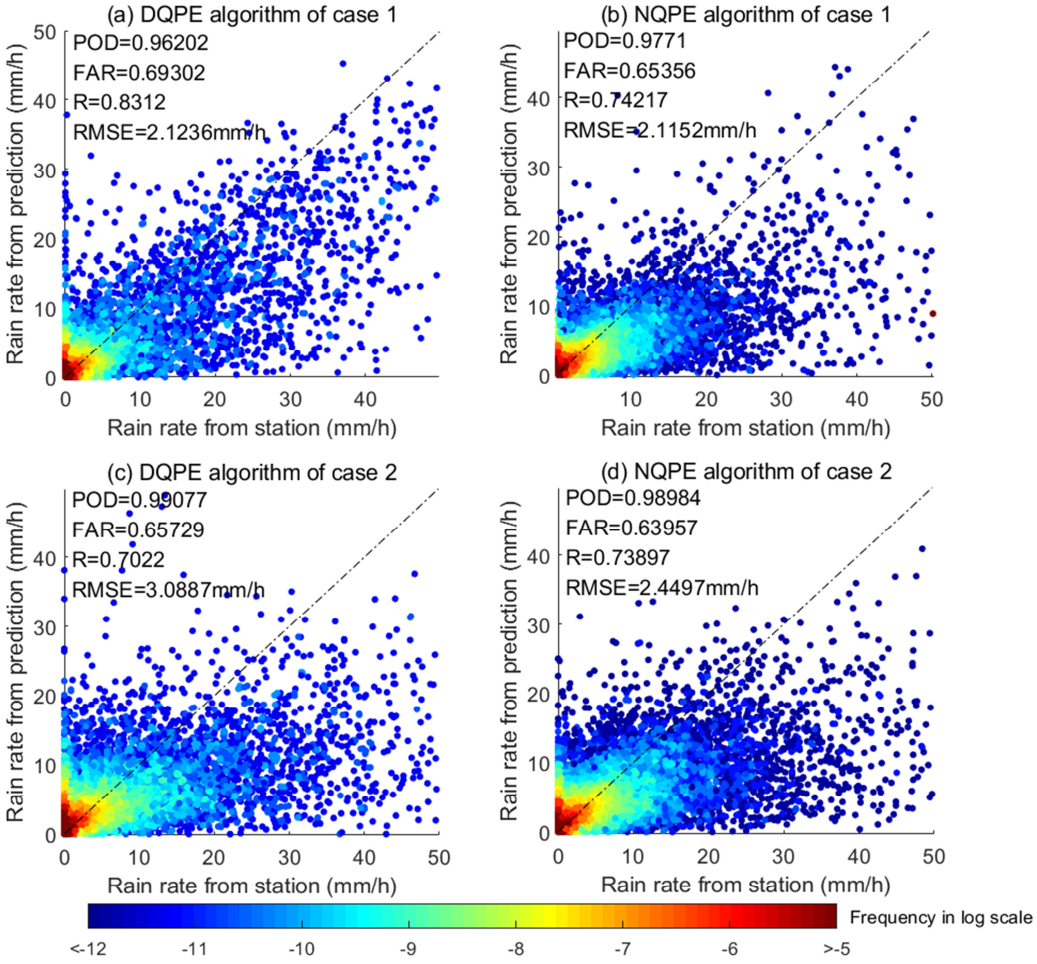

Figure S1: Comparison of the precipitation measured by high-density automatic stations and that predicted by the QPE algorithm: (a) DQPE algorithm of case 1; (b) NQPE algorithm of case 1; (c) DQPE algorithm of case 2; (d) NQPE algorithm of case 2

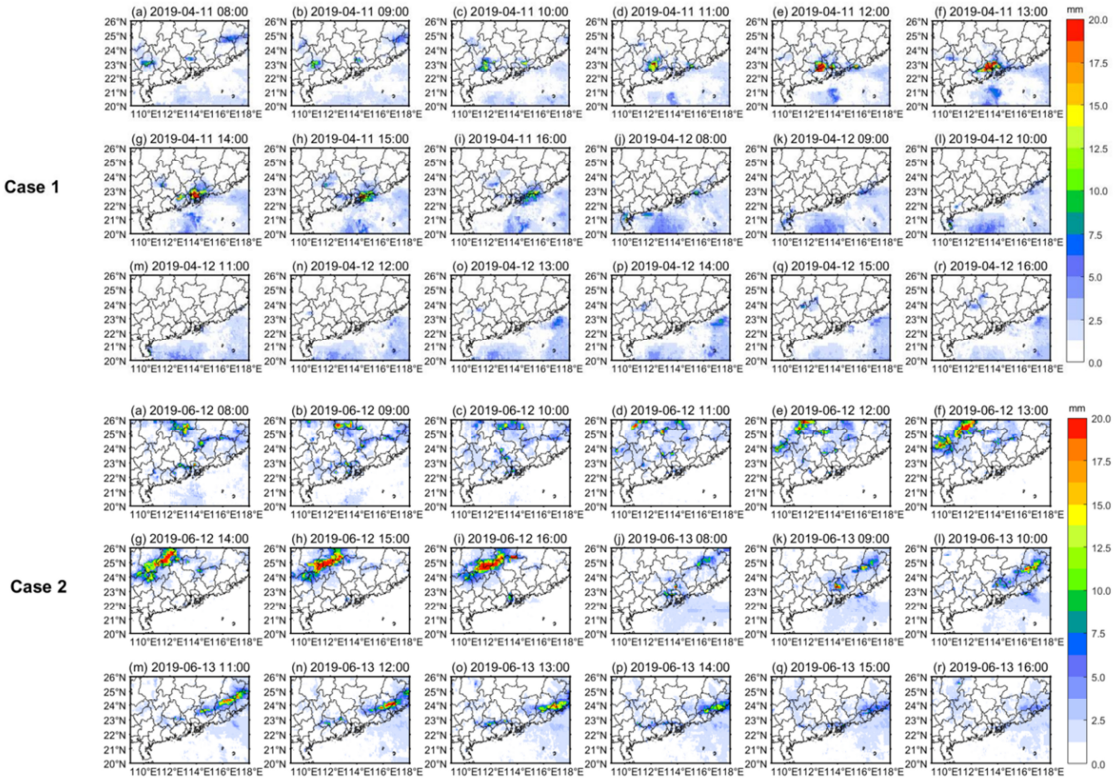

Figure S2: Predicted precipitation of the DQPE algorithm: Case 1: (a–i) at 0800–1600 BJT on April 11; (j–r) at 0800–1600 BJT on April 12. Case 2: (a–i) at 0800–1600 BJT on June 12; (j–r) at 0800–1600 BJT on June 13.

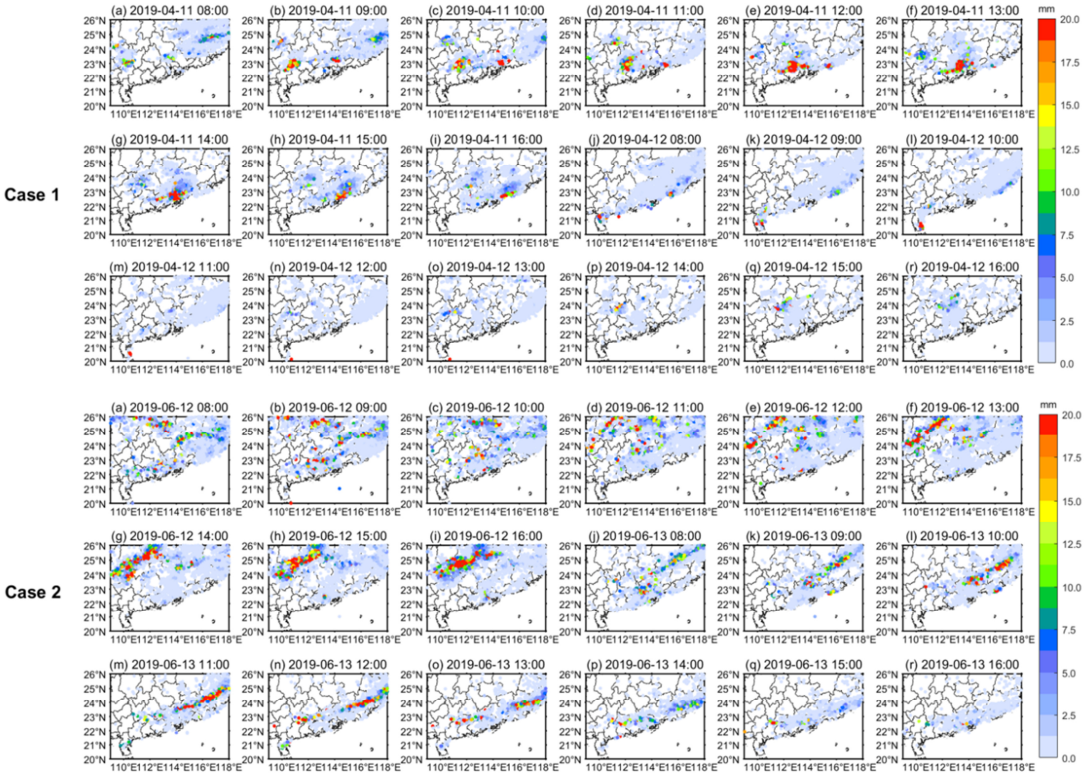

Figure S3: Actual precipitation based on the high-density automatic stations: Case 1: (a–i) at 0800–1600 BJT on April 11; (j–r) at 0800–1600 BJT on April 12. Case 2: (a–i) at 0800–1600 BJT on June 12; (j–r) at 0800–1600 BJT on June 13.

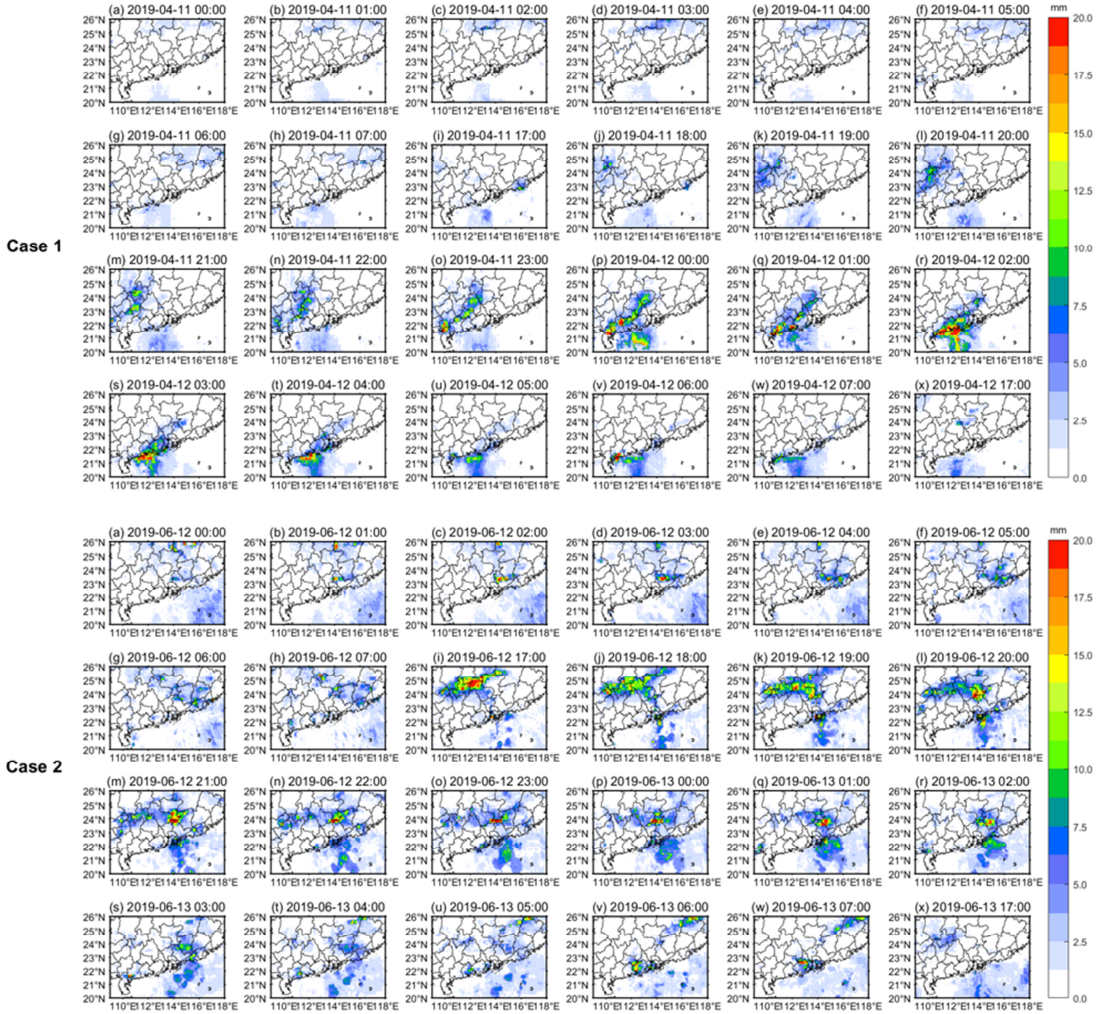

Figure S4: Predicted precipitation of the DQPE algorithm: Case 1: (a–h) 0000–0700 BJT on April 11, (i–o) 1700–2300 BJT on April 11, (p–w) 0000–0700 BJT on April 12, and (x) 1700 BJT on April 12. Case 2: (a–h) 0000–0700 BJT on June 12, (i–o) 1700–2300 BJT on June 12, (p–w) 0000–0700 BJT on June 13, and (x) 1700 BJT on June 13.

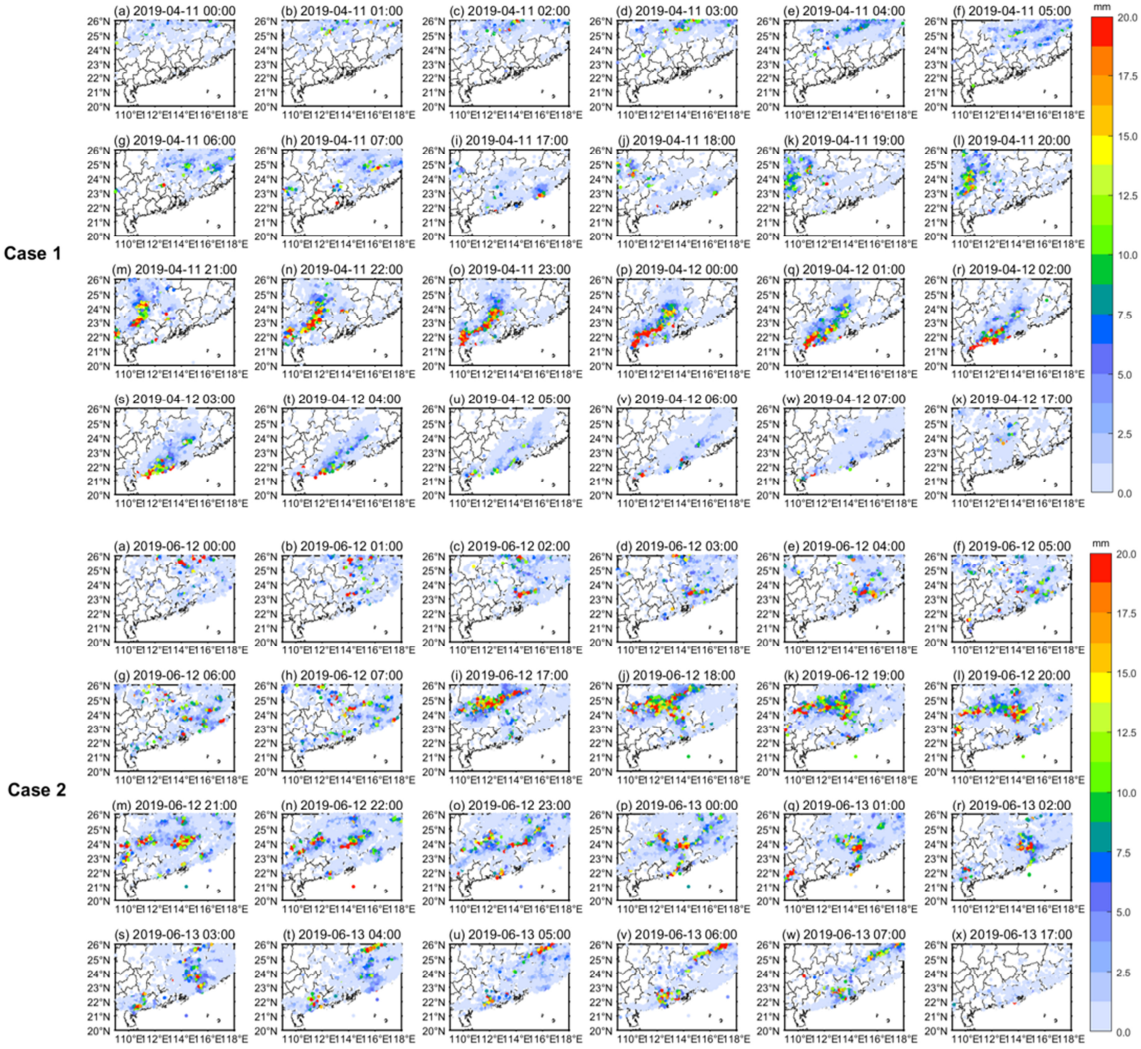

Figure S5: Actual precipitation based on the high-density automatic stations: Case 1: (a–h) 0000–0700 BJT on April 11, (i–o) 1700–2300 BJT on April 11, (p–w) 0000–0700 BJT on April 12, and (x) 1700 BJT on April 12. Case 2: (a–h) 0000–0700 BJT on June 12, (i–o) 1700–2300 BJT on June 12, (p–w) 0000–0700 BJT on June 13, and (x) 1700 BJT on June 13.

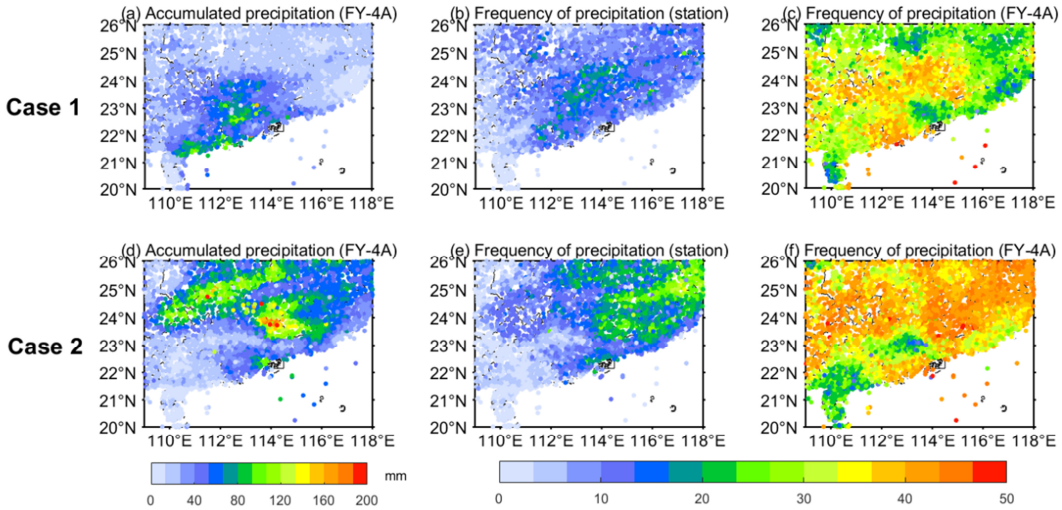

Figure S6: Spatial distribution of accumulated precipitation: (a) accumulated precipitation predicted by the QPE algorithm in case 1; (b) actual precipitation frequency observed by high-density automatic stations in case 1; (c) precipitation frequency predicted by the QPE algorithm in case 1; (d) accumulated precipitation predicted by the QPE algorithm in case 2; (e) actual precipitation frequency observed by high-density automatic stations in case 2; (f) precipitation frequency predicted by the QPE algorithm in case 2.

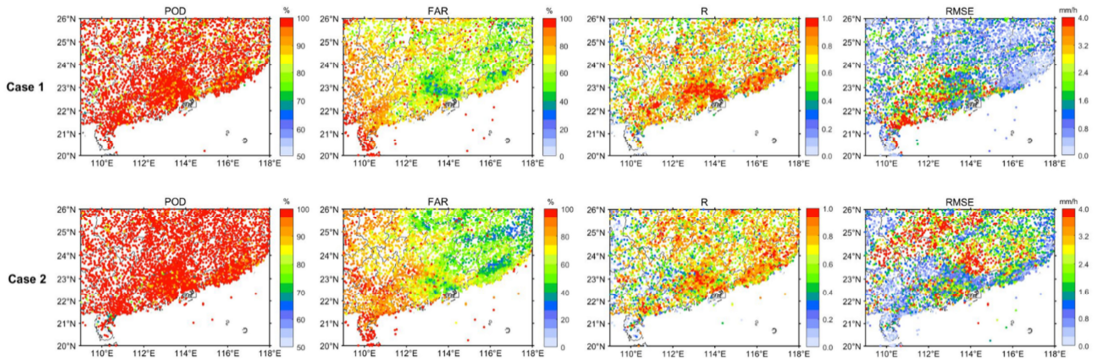

Figure S7: Spatial distribution of evaluation indicators of the QPE algorithm for all stations: (a) POD in case 1; (b) FAR in case 1; (c) R in case 1; (d) RMSE in case 1; (e) POD in case 2; (f) FAR in case 2; (g) R in case 2; (h) RMSE in case 1.

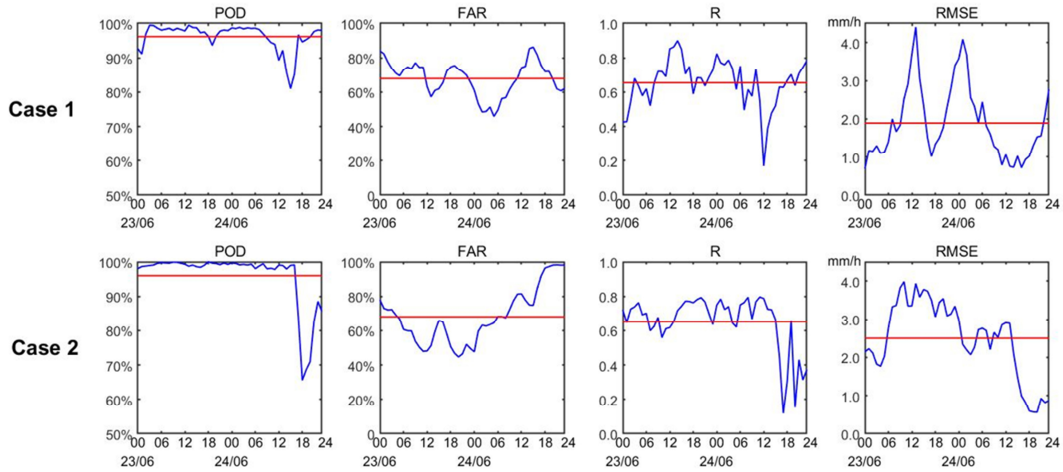

Figure S8: Time series of evaluation indicators of the QPE algorithm for all stations at each time: (a) POD in case 1; (b) FAR in case 1; (c) R in case 1; (d) RMSE in case 1; (e) POD in case 2; (f) FAR in case 2; (g) R in case 2; (h) RMSE in case 1.